Mechanical and Corrosion Protection Properties of a Smart Composite Epoxy Coating with Dual-Encapsulated Epoxy/Polyamine in Carbon Nanospheres

Haddadi, S. A.; Ramazani, A. S.A.; Mahdavian, M.; Taheri, P.; Mol, J. M.C.

DOI
10.1021/acs.iecr.8b06306

Publication date
2019

Document Version
Final published version

Published in
Industrial and Engineering Chemistry Research

I&EC research
Industrial & Engineering Chemistry Research

Article

Cite This: Ind. Eng. Chem. Res. 2019, 58, 3033−3046

pubs.acs.org/IECR

Mechanical and Corrosion Protection Properties of a Smart Composite Epoxy Coating with Dual-Encapsulated Epoxy/Polyamine in Carbon Nanospheres

S. A. Haddadi,[†] A. Ramazani S. A.,[*,†] M. Mahdavian,[‡,*] P. Taheri,[§] and J. M. C. Mol[§]

[†]Chemical and Petroleum Engineering Department, Sharif University of Technology, P. O. Box 11155-9465, Tehran, Iran
[‡]Surface Coating and Corrosion Department, Institute for Color Science and Technology, P. O. Box 54-16765, Tehran, Iran
[§]Department of Materials Science and Engineering, Delft University of Technology, 2628CD Delft, The Netherlands

ABSTRACT: Carbon nanocapsules doped separately with epoxy and polyamine were used to fabricate an epoxy nanocomposite coating. Carbon nanospheres with dual-encapsulated epoxy/polyamine were dispersed uniformly in the epoxy resin at concentrations of 2, 5, and 10 wt %. The mechanical properties of the nanocomposites were studied by tensile testing and scratch hardness measurements. Furthermore, nanocomposites were applied on mild steel substrates, and their corrosion protection and barrier performance were evaluated using electrochemical impedance spectroscopy (EIS). Adhesion loss measurements of coatings after 240 h exposure to 3.5 wt % NaCl solution were performed by pull-off adhesion testing. Also, the buried steel/polymer interface was studied in situ using attenuated total reflection Fourier transform infrared spectroscopy in the Kretschmann geometry. The results showed that both mechanical and corrosion protection properties of the prepared nanocomposites are enhanced as compared to the baseline epoxy coating and improved with the concentration of doped carbon nanocapsules. Maximum mechanical and corrosion protection properties were achieved in the case of 10 wt % doped carbon nanocapsules as a result of active intermolecular interactions between the epoxy and polyamine chains of the coating matrix and amine groups grafted on the surface of carbon capsules.

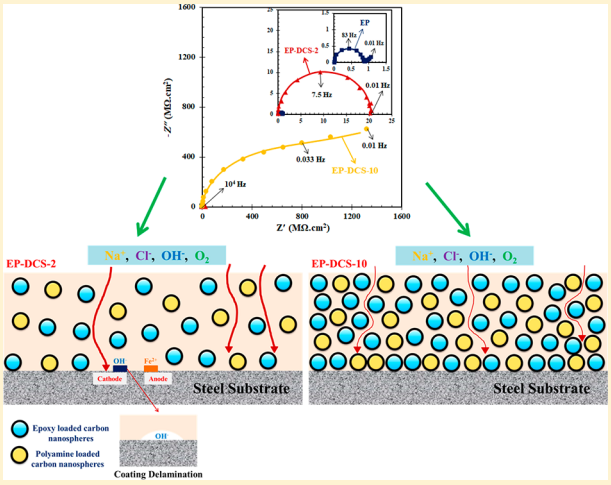

1. INTRODUCTION

Polymeric materials such as epoxies and polyurethanes are widely used as organic coatings to protect metallic structures against corrosion.[1−3] Covering the surface of metals with organic coatings provides a physical barrier between the surface of the metallic substrate and a corrosive environment.[4,5] Among all organic coatings, epoxy coatings are known for their cost-efficiency, excellent adhesion, easy accessibility and applicability, mechanical properties, and electrical insulation.[6−8] However, like other polymers, epoxy is permeable to environmental components such as water, oxygen, hydroxyl, and aggressive chloride ions resulting in a reduced corrosion protection.[4,9] Upon exposure of the coating systems to corrosive media, the electrolyte penetration to the metal−polymer interface may lead to adhesion loss, coating delamination, and blistering.[2,4,9]

In recent decades, many attempts have been undertaken by researchers to enhance the corrosion protection and barrier performance of epoxy coatings against corrosive species.[10] Modification of the epoxy with active and nonactive silane precursors such as aminopropyltrimethoxy[11] and bis-1,2-(triethoxysilyl)ethane[12,13] on AA2024 alloy showed that the coating adhesion and corrosion protective performance of epoxy coatings were enhanced remarkably in the presence of the organosilanes. Moreover, micro-/nanopigments, fillers, and other additives have been incorporated in epoxy coatings to enhance their durability and corrosion protective performance.[14,15] The results demonstrated that fillers and pigments such as glass flake,[16] zinc oxide,[17] lamellar aluminum fillers,[18] inhibitive and sacrificial pigments, e.g., zinc phosphates[19,20] and zinc[17] enhanced the corrosion protection of the polymer system in corrosive media. Among these fillers and pigments, nanofillers physically block micropores and cavities of the polymer matrix and reduce the penetration of the electrolyte through the coating and consequently to the metal/coating interface due to a higher surface area compared to the microsized fillers conventionally used.[2,21]

The barrier and corrosion protective properties of various types of nanofillers such as ZrO_2,[22] Ag_2O,[23] SiO_2,[24] Al_2O_3,[25] ZnO,[26] Fe_2O_3,[27] Cr_2O_3,[28] TiO_2,[29,30] Au,[31] and clay[32] incorpo-

Received: December 20, 2018
Revised: February 5, 2019
Accepted: February 7, 2019
Published: February 7, 2019

DOI: 10.1021/acs.iecr.8b06306
Ind. Eng. Chem. Res. 2019, 58, 3033−3046

Table 1. Chemical Composition of ST-12 Plates

element	Si	P	S	C	Cu	other	Fe
wt %	0.016	0.005	0.0086	0.037	0.065	0.13	balance

rated in epoxy coatings applied on steel substrates have been studied in saline aqueous solutions. It was shown that epoxy coatings offer better barrier and corrosion protective properties in the presence of these nanoparticles. Carbon-based nanostructures, e.g., carbon nanotubes,[33] nanodiamond,[34] fullerene,[35] graphene,[33] graphene oxide,[2] and carbon spheres,[36] have been studied widely to fabricate nanocomposite coatings with enhanced chemical, physical, mechanical, and corrosion protective properties. The barrier and corrosion protection properties of the organic coatings are enhanced by introducing micro-/nanocontainers doped with active agents such as corrosion inhibitors, catalysts, and film-forming agents, such as curable resins, reactive monomers, oil-based healing agents, and organofunctional silanes in the polymer matrix.[36,37] The embedded micro-/nanocontainers, e.g., graphene-based nanostructures, promote the overall mechanical strength of the matrix and the timely release of the doped active agents via capillary forces within the damaged areas. This, in turn, recovers the damaged region by healing and consequently active corrosion protection.

Direct incorporation of these active agents in the polymer matrix may cause structural defects and reduce the protection efficiency of the coatings due to their effects on the curing reactions.[37] To overcome these drawbacks and to prolong the durability of the polymer matrix, encapsulation of active agents in micro-/nanoreservoirs can both provide barrier properties and control the release of agents at coating defects on-demand.[36,38,39] Among the above-mentioned pigments and nanofillers, almost none of them have interior spaces, cavities, and porous structure for encapsulation of these active agents. Consequently, porous and hollow structures such as halloysites,[40] montmorillonites,[41] bentonites,[42] zeolites,[43] layered double hydroxides,[39] polymeric layer-by-layer assembled structures[44] and other hollow nanocontainers[37,45] are used as hosts for active agents.

Yi et al.[46] and Jin et al.[47] reviewed the effects of epoxy/amine dual core polymeric microcapsules on the self-healing properties of an epoxy resin. They reported that release of epoxy and amine active agents could heal coating defects and prevent coating delamination. The same results were obtained for an epoxy coating containing double stimuli-responsible urea−formaldehyde microcapsules doped separately with linseed oil and azole components by Leal et al.[48] and Siva et al.[45] The effects of epoxy microcapsules and polyaniline nanofibers on the self-healing and protective properties of the epoxy coating were evaluated by Zhang et al.[49] They showed that the highest protection and self-healing performance was achieved by epoxy microcapsules and polyaniline nanofibers incorporated in the epoxy coating.

In the previous work, graphene-based carbon hollow spheres doped with corrosion inhibitors were fabricated to study the pH-triggered release of inhibitors from carbon containers to the saline solution.[36]

The aim of this study is to evaluate the effects of epoxy/polyamine dual-encapsulated carbon nanospheres on the mechanical, barrier performance, and corrosion protection properties of the intact epoxy coatings containing different concentrations of doped carbon capsules. EIS measurements were used to study the corrosion protection performance of the nanocomposites applied on steel substrates. The adhesion strength of the coating systems before and after 240 h exposure to 3.5 wt % NaCl solution was assessed by pull-off adhesion tests. The mechanical properties of epoxy nanocomposites were investigated using tensile testing and scratch hardness measurements.

2. EXPERIMENTAL SECTION

2.1. Materials. Epikote 828 epoxy resin and Epikure F205 polyamine hardener were purchased from Kian Resin Co., Iran. ST-12 steel plates were obtained from Foolad Mobarake Co., Iran. Table 1 shows the chemical composition (wt %) of the steel plates. The surface of steel samples with 100 mm × 80 mm × 1 mm dimensions were polished using 400, 800, and 1200 grade SiC papers and then cleaned with acetone (98%, Mojallali Co., Iran) prior to coating application. Commercially pure iron sheets (99.95%) were purchased from Goodfellow.

2.2. Synthesis of Epoxy/Polyamine Dual-Encapsulated Carbon Spheres. A silica templating method was used to synthesize carbon hollow spheres (CHSs) as reported in detail in our previous work.[36] For this purpose., silica templates were synthesized by the Stober method. Then, silica core/polysaccharide shell nanostructures were fabricated using a hydrothermal method. Silica core/carbon shell nanostructures were obtained by high-temperature carbonization of silica core/polysaccharide shell nanostructures under an inert atmosphere. An acid treatment method was employed for silica templates removal. Before loading of epoxy and polyamine in the synthesized CHSs, the surface of CHSs was chemically modified by (aminopropyl)triethoxysilane (APTES) to enhance their compatibility with the epoxy matrix. Encapsulation of epoxy and polyamine agents in separate CHSs was performed by preparation of dilute suspensions of CHSs in epoxy/acetone and polyamine/acetone solutions in a vacuum chamber as discussed in detail in literature.[46] In the present work, the epoxy and polyamine loaded carbon spheres were denoted as Ep-DCS and Am-DCS, respectively. The core contents of Ep-DCSs and Am-DCSs were evaluated using a solvent extraction method. For this purpose, a bath sonicator (James SONIC 6MX, 240 W and 37 kHz) was used to disperse a certain amount of doped carbon capsules (W_{DCS}) in acetone for 12 h. Then, the extracted carbon capsules were washed three times by acetone and dried in an oven at 60 °C for 24 h. The final extracted carbon capsules weight (W_{CHS}) was measured and the core content of doped carbon capsules was calculated using eq 1.

$$\text{core content of doped carbon capsules}/\% = \frac{W_{DCS} - W_{CHS}}{W_{DCS}} \times 100 \quad (1)$$

After calculation of the core contents of Ep-DCSs and Am-DCSs by eq 1, the epoxy and polyamine contents doped in carbon capsules were about 35 and 39% based on the weight of Ep-DCSs and Am-DCSs, respectively.

2.3. Sample Preparation. *2.3.1. Mechanical Characterization.* In order to investigate the mechanical properties of the prepared nanocomposite coatings, the uncured nanocomposites were cast in a silicon rubber mold according to ASTM D 638 and kept at ambient conditions (24 ± 1 °C and 30 ± 2% relative humidity (RH)) for 24 h. Then, the molded nanocomposites

DOI: 10.1021/acs.iecr.8b06306
Ind. Eng. Chem. Res. 2019, 58, 3033−3046

were postcured for 1 h in a furnace at 110 °C. The nanocomposite sheets with 60 mm × 40 mm × 3 mm dimensions were prepared by the same procedure as that for the scratch hardness measurement. Triplicates were prepared for each tensile test and scratch hardness measurement.

2.3.2. EIS and Pull-off Experiments. To prepare epoxy nanocomposite coatings, 0, 2, 5, and 10 wt % of Ep-DCSs were uniformly dispersed in the epoxy resin using a bath sonication for 20 min. Then, 0, 1, 2.5, and 5 wt % Am-DCSs were dispersed in the polyamine hardener by the same procedure to ensure the complete reaction between epoxy and polyamine agents in a stoichiometric ratio (2:1, w/w). Next, the prepared epoxy resins containing EP-DCSs were mixed with the proper polyamine hardeners containing Am-DCSs in a stoichiometric ratio, and then the prepared nanocomposites containing 0, 2, 5, and 10 wt % Ep-DCS were labeled as EP, EP-DCS-2, EP-DCS-5, and EP-DCS-10, respectively. All epoxy coatings were applied on steel substrates using a four-sided film applicator (Elcometer 3520 Baker) at a wet thickness of 90 ± 5 μm. The coated steel samples were kept at ambient temperature (24 ± 1 °C and 30 ± 2% RH) and then postcured for 1 h in a furnace at 110 °C. The dry thickness of samples after curing was determined by an Elcometer 456 and was 65 ± 5 μm. For EIS measurements, the coated steel plates were cut into 100 mm × 40 mm × 1 mm dimensions and all measurements were carried out on 1 cm^2 of the coatings. A hot melt beeswax−colophony mixture was used to seal the remaining area of each sample.

2.4. Characterization. The morphology of the fabricated carbon spheres before and after removal of silica templates and the sonication process were evaluated using FE-SEM (Jeol, JSM-6500F, Japan). To ensure the silica template removal, energy-dispersive X-ray spectroscopy (EDS; Oxford Instrument, United Kingdom) was conducted before and after the acid treatment process by elemental line scans of carbon (C), oxygen (O), and silicon (Si) on silica core/carbon shell structures. FE-SEM analysis of the fracture surface of nanocomposites after the tensile test was also performed to study the dispersion of doped carbon spheres in the epoxy matrix.

A universal tensile machine (Zwick, Roell-Z010, Germany) was used to evaluate the effects of Ep-DCSs and Am-DCSs on the mechanical properties of epoxy coatings at ambient conditions (24 ± 1 °C and 30 ± 2% RH) at a loading rate of 1 mm min^{-1}. The scratch hardness values of the prepared nanocomposites were determined according to ASTM G171-03 by a scratch hardness tester (Sharif-Azma, Iran). The width of the scratch tracks of the samples was measured by an optical microscope (Olympus bx51, Japan) at three different locations. All measurements were carried out under a 5 N normal load and 1.5 mm s^{-1} scratch rate. The scratch hardness values were calculated by eq 2:[50,51]

$$H_S = \frac{8F_N}{\pi b^2} \tag{2}$$

where F_N and b are the applied normal load and width of the scratch track, respectively.

The adhesion strength of all epoxy coatings to the steel substrates before and after 240 h exposure to 3.5 wt % NaCl solution was determined by a PosiTest pull-off adhesion tester (DEFELSKO). For this purpose, a two-part transparent adhesive (Huntsman Advanced Materials, Germany) was used to glue the aluminum dollies (20 mm in diameter) on the coatings surface. Then, the samples were placed in ambient temperature for 24 h for full curing of the glues. Finally, the coating around the dollies was slotted and the dollies were then pulled at a 10 mm min^{-1} normal speed until the coatings detached from the steel substrates. The pull-off adhesion tests were performed three times at 24 ± 1 °C and 30 ± 2% RH according to ASTM D4541 standard to study the reproducibility of measurements.

To study the adhesion mechanism of nanocomposite coatings at the steel/coating interface, an ATR-FTIR technique was used in Kretschmann geometry. For this purpose, an FTIR spectrometer (Thermo SCIENTIFIC, NICOLET 6700, USA) equipped with a mercury−cadmium−telluride liquid-nitrogen-cooled detector and a Harrick Seagull multipurpose reflection accessory was employed. Before the measurement, the surface of internal reflection element (IRE) hemispheres (Harrick Scientific Products Inc., 25 mm in diameter) made of germanium (Ge) and zinc selenium (ZnSe) was coated by a thin film of pure iron (25 nm in thickness) by means of a high-vacuum evaporation (Balzers BAE 250, USA) coating system. Then, the coated GE IRE was attached in the accessory, and uncured EP and EP-DCS-10 coatings were applied on the surface of the Ge IRE (500 μm in thickness). In situ FTIR spectra of curing coatings were recorded every 20 s until the applied coating was fully cured. The same process was repeated for the coated ZnSe IRE.

The effects of incorporation of Ep-DCSs and Am-DCSs on the corrosion protective ability of the epoxy coatings were evaluated at different immersion times (5, 25, and 50 days) by EIS tests. All EIS measurements were conducted in a three-electrode cell including saturated Ag/AgCl, platinum, and coated steel samples as the reference, counter, and working electrodes, respectively. CorrTest (CS 350, China) was employed to measure the EIS data at open circuit potential (OCP) in the frequency range of 10 mHz to 10 kHz and at 10 mV (peak to zero) amplitude. The measurements were performed in triplicate to check the reproducibility of the data.

3. RESULTS AND DISCUSSION

3.1. Carbon Capsules Characterization. FE-SEM analysis was used to assess the effect of applied stresses during the sonication method on mechanical properties of carbon shells. FE-SEM images of the carbon capsules before and after sonication in acetone are shown in Figure 1. The morphology of the synthesized hollow nanostructures originates from the final shape of the used templates in the soft and hard templating processes performed. As shown in Figure 1a,c, the carbon capsules before and after removal of silica templates are spherical with an average diameter of 300 ± 50 nm. Also, after silica template removal, the spherical shape of carbon shells was retained, which indicates adequate mechanical properties and dimensional stability of the carbon shells. After the sonication process, the large agglomerations of silica core/carbon shells and CHSs were broken into smaller agglomerations with less than 20 nanospheres. Furthermore, no changes in the spherical morphology of capsules and fragments of carbon shells were observed. This indicates that the applied stresses during dispersion of the doped carbon capsules in the epoxy matrix did not lead to mechanical failure of the carbon shells.

EDS elemental line-scan analysis was performed on carbon capsules before and after extraction of the silica templates via the acid treatment to evaluate the effects of template removal. Figure 2a shows that before template removal, C, O, and Si elements can all be found on silica core/carbon shell structures. Higher silica core/carbon shell weight ratios have resulted in the higher

DOI: 10.1021/acs.iecr.8b06306
Ind. Eng. Chem. Res. 2019, 58, 3033−3046

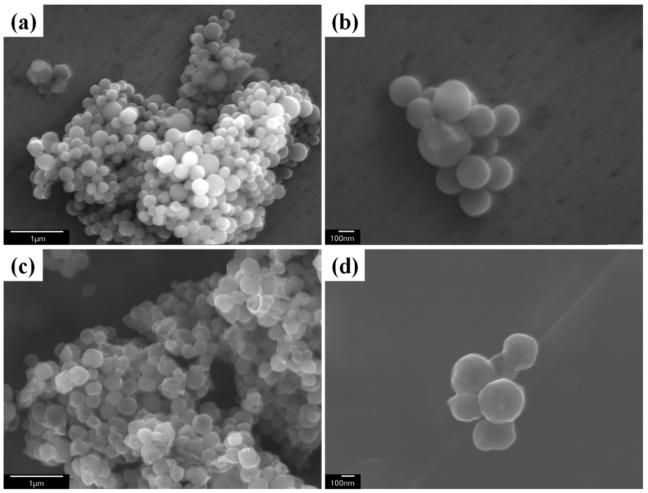

Figure 1. FE-SEM images of the carbon capsules before and after removal of silica templates (a and c) and sonication process (b and d), respectively.

content of O and Si elements as compared to C. After the acid treatment, the concentrations of O and Si elements were considerably lower, and the higher concentration of C in comparison with O and Si elements showed formation of hollow carbon shells (see Figure 2b).

3.2. Mechanical Characterization of Nanocomposite Coatings. The effects of addition of doped carbon capsules on the mechanical properties of the epoxy were investigated using a tensile test. The typical stress−extension curves of different samples, as well as the extracted data from stress−extension curves including tensile strength, tensile extension, Young's modulus, and toughness, are presented in Figure 3. As shown in Figure 3a,b, the tensile strengths for all nanocomposites were enhanced in the presence of doped carbon capsules and reached from 32 to 74 MPa for EP and EP-DCS-10, respectively. Addition of solid rigid fillers such as graphene-based carbon capsules with good mechanical properties makes the soft epoxy matrix less flexible, enhancing the tensile strength and decreasing the elongation at failure of nanocomposite samples. During the tensile test, the polymer chains of the matrix have considerable segmental mobility and they can slip and slide leading to the disentanglement of the polymer chains.[22] However, the segmental mobility of the epoxy chains decreases with the placement of carbon capsules between the epoxy chains, resulting in a decrease of the elongation at failure of about 75% for EP-DCS-10 compared to an EP sample due to the created steric hindrance by the doped carbon capsules.

It can be inferred that grafted NH_2 groups on the surface of carbon capsules can react with epoxide groups of epoxy chains (see section 3.4) and form a strong filler/polymer interface with enhanced mechanical properties around carbon capsules. Consequently, the applied stresses can properly transfer from the epoxy matrix to carbon capsules by the formation of this strong interface. Thus, carbon capsules can play a role of alternative cross-linkers in the epoxy matrix restricting the segmental mobility of epoxy chains, thereby enhancing the tensile strength of the matrix and increasing the Young's modulus as shown in Figure 3c. The area under the stress−extension curve is considered as toughness which is equal to the energy content absorbed by the sample before mechanical failure.[52] Increasing toughness of epoxy samples in the presence of carbon capsules indicates that the samples containing higher concentrations of doped carbon capsules can absorb more

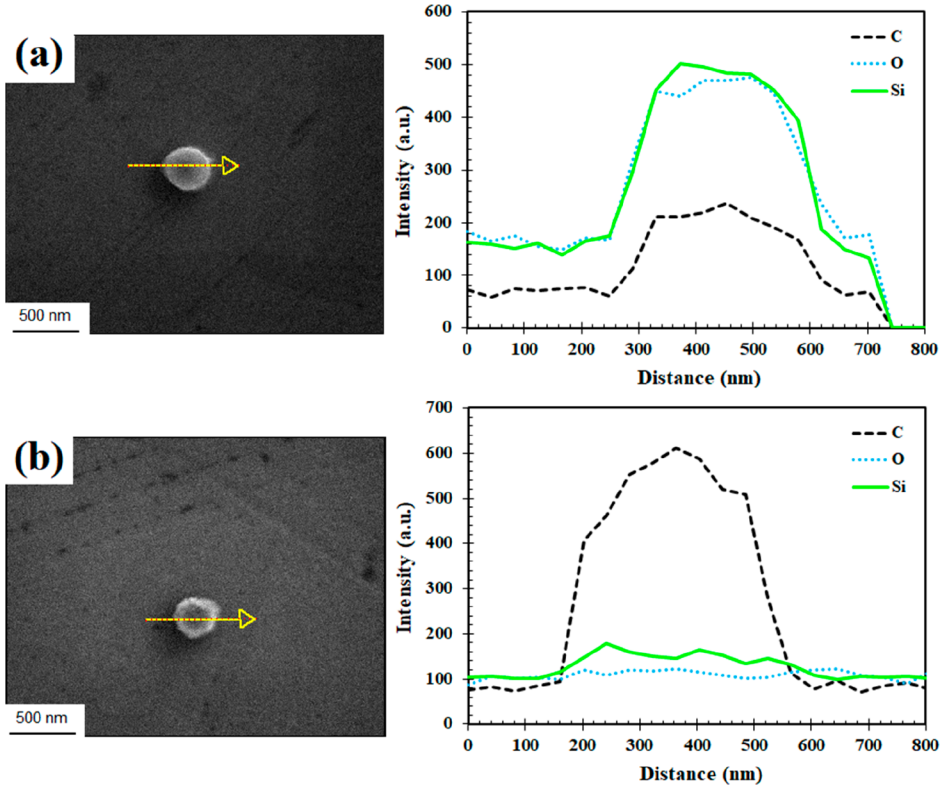

Figure 2. FE-SEM images and EDS elemental line-scan plots of carbon capsules before (a) and after (b) removal of silica templates.

DOI: 10.1021/acs.iecr.8b06306
Ind. Eng. Chem. Res. 2019, 58, 3033−3046

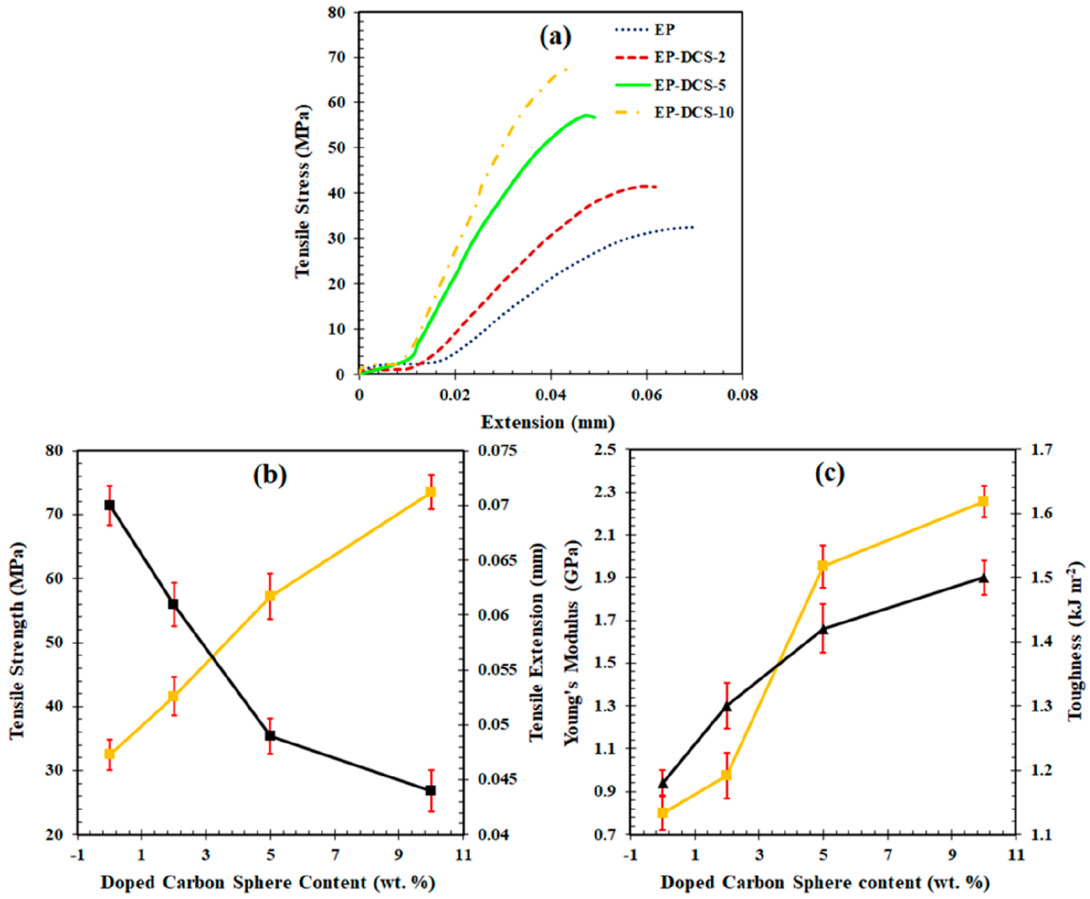

Figure 3. Typical stress−extension curves (a), tensile strength and extension (b), Young's modulus and toughness (c), versus the concentration of doped carbon capsules.

energy before mechanical failure due to good compatibility and dispersion of carbon capsules in the epoxy matrix.

Dispersion of carbon capsules in the epoxy matrix for EP-DCS-2 and EP-DCS-10 samples was studied by FE-SEM analysis from the fracture surface of nanocomposite samples after tensile testing as illustrated in Figure 4. It can be seen that carbon capsules were dispersed uniformly in the epoxy matrix. This observation indicates good compatibility of amino-functionalized carbon capsules with the epoxy matrix leading to uniform dispersion and distribution with few agglomerations. As we discussed in our previous work,[36] synthesis of carbon hollow spheres at high temperature (~900 °C) results in carbon capsules without functional groups at their surface. Addition of these unmodified nanostructures to the epoxy matrix leads to the formation of agglomerates and aggregates due to the higher surface energy of carbon capsules before surface modification.[53,54] These agglomerates and aggregates initiate locations of stress concentration in the epoxy matrix, and the mechanical failure may occur at lower stresses. Amino functionalization of carbon capsules makes them more hydrophobic.[53,55] As a result, the epoxy matrix can wet the surface of carbon capsules well and construct a strong interface around carbon capsules due to their higher compatibility with the epoxy matrix after surface modification resulting in improved mechanical properties and better dispersion.

To compare the scratch hardness of different coatings, optical images and the width of scratch tracks on the coating surfaces are shown in Figure 5. Values of scratch hardness calculated by eq 2 are presented in Table 2.

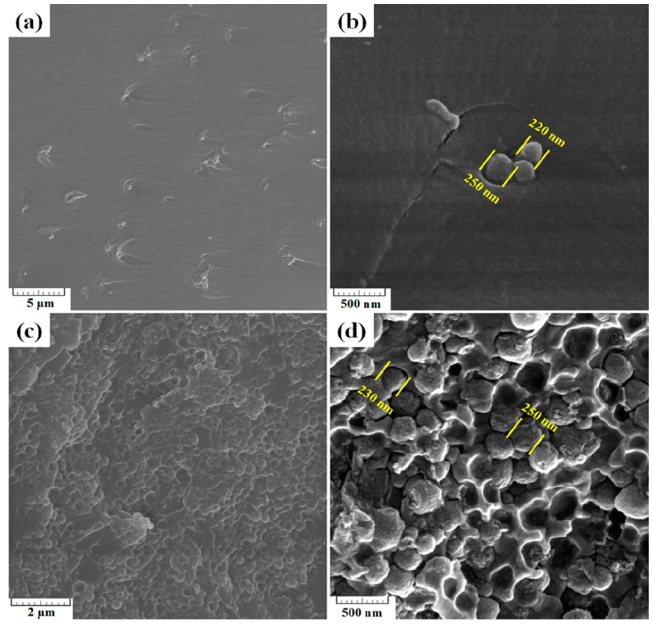

Figure 4. FE-SEM images of the fracture surface of EP-DCS-2 (a, b) and EP-DCS-10 (c, d) nanocomposites after tensile testing at different magnifications.

As shown in Figure 5 and Table 2, the widths of scratch tracks were reduced from 196 to 166 μm with the addition of carbon capsules for the EP-DCS-10 coating compared to EP coating. As

DOI: 10.1021/acs.iecr.8b06306
Ind. Eng. Chem. Res. 2019, 58, 3033−3046

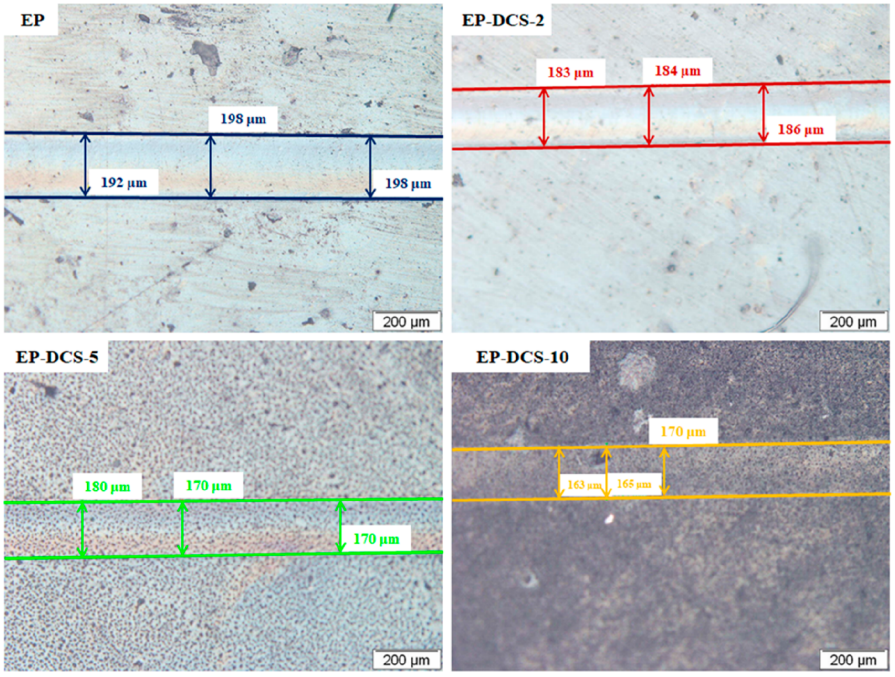

Figure 5. Optical images and widths of scratch tracks of the different coating surfaces.

Table 2. Values of Scratch Harness for Different Coatings

sample	F_N (N)	b (mm)	H_s (MPa)
EP	5	196.0 ± 2.8	331.6
EP-DCS-2	5	184.3 ± 1.3	375.0
EP-DCS-5	5	173.3 ± 4.7	424.0
EP-DCS-10	5	166.0 ± 2.9	462.3

reported elsewhere,[56] the presence of graphene-based materials even at low concentrations could offer enhanced reinforcement of the soft polymeric materials due to their favorable physical and chemical properties and superior mechanical strength. Consequently, the scratch hardness and mechanical properties of the epoxy coating increase with the concentration of graphene-based capsules as shown in Table 2. Addition of surface modified carbon capsules in the epoxy matrix not only improved the mechanical properties of the epoxy bulk but also enhanced the scratch hardness of epoxy coating against applied stresses and indentation of sharp objects.

3.3. Adhesion Loss Measurements. The adhesion strength of different coatings prior to and after 240 h exposure to 3.5 wt % NaCl solution was determined using pull-off testing shown in Figure 6. Adhesion loss values of different coatings were calculated according to eq 3.

$$\text{adhesion strength loss}/\% = \frac{\Gamma_D - \Gamma_W}{\Gamma_D} \times 100 \quad (3)$$

where Γ_D and Γ_W are the dry and wet adhesion strengths of the coating, respectively. As shown in Figure 6, the wet adhesion strength of the EP sample is much lower than the dry adhesion strength as a result of the electrolyte diffusion into the coating in the absence of the doped carbon capsules. In addition, values of the wet adhesion strength of all epoxy coatings were lower than

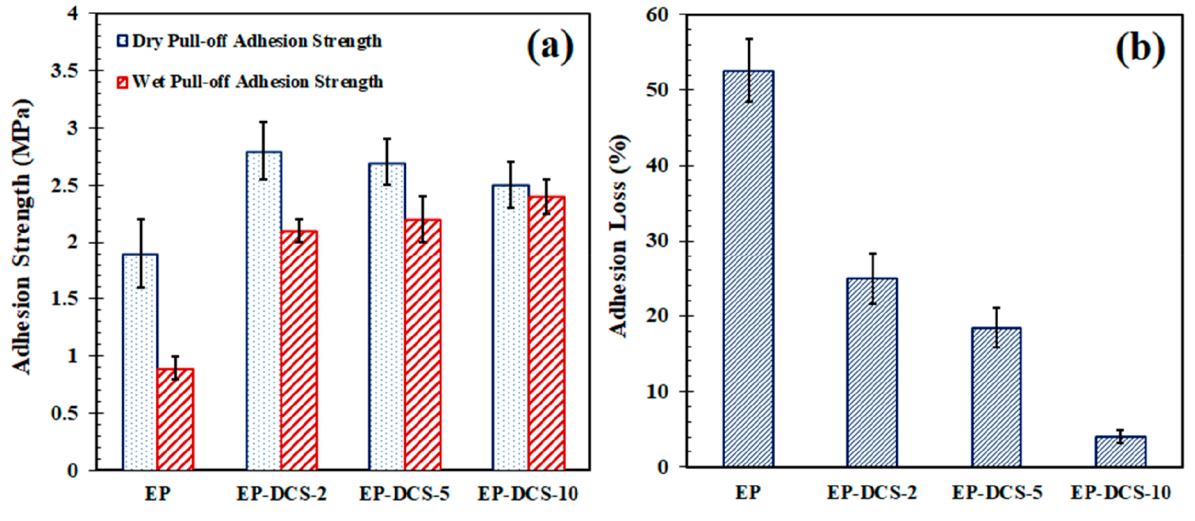

Figure 6. Values of the wet and dry adhesion strength (a) and adhesion loss (b) of different coatings.

DOI: 10.1021/acs.iecr.8b06306
Ind. Eng. Chem. Res. 2019, 58, 3033−3046

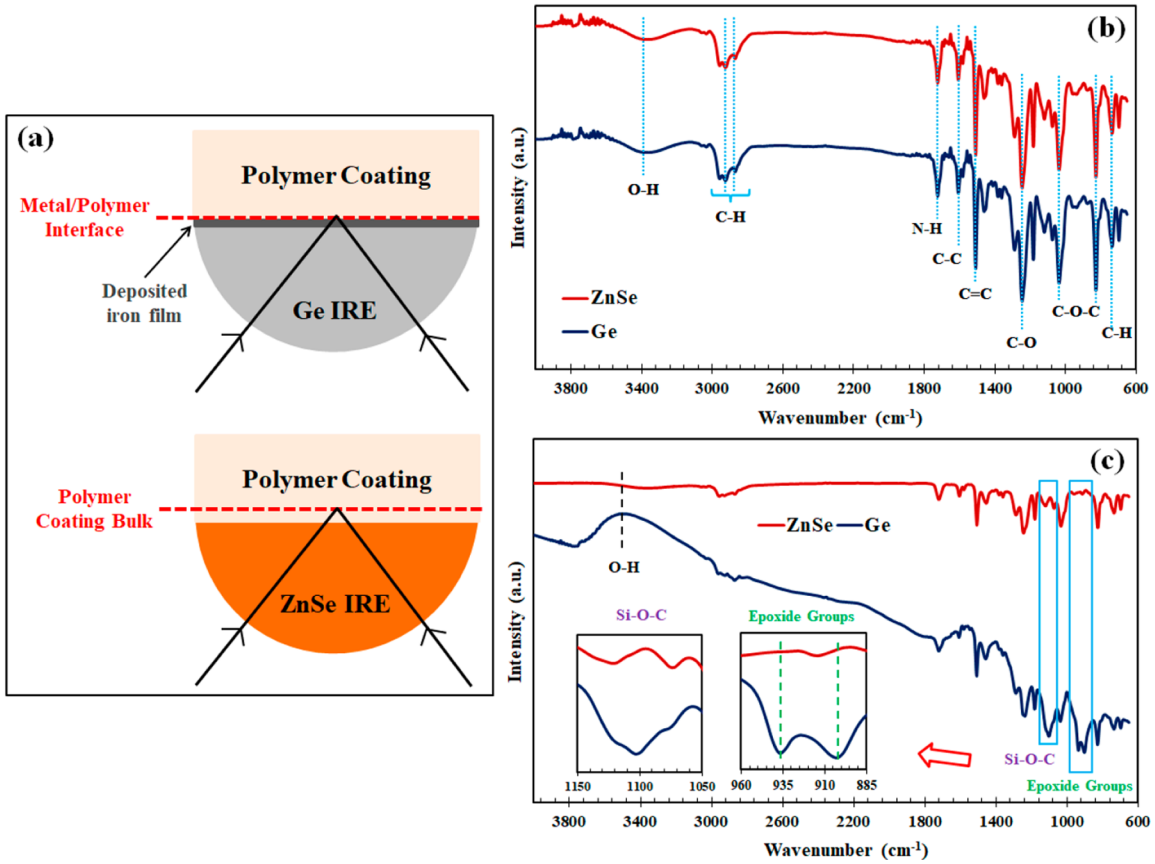

Figure 7. In situ evaluation of the polymer−metal interfaces and polymer groups by Ge and ZnSe IREs (a) and in situ ATR-FTIR spectra of fully cured EP (b) and EP-DCS-10 (c) coatings detected by Ge and ZnSe IREs.

those of the dry adhesion strength. This can be due to the electrolyte diffusion to the metal/coating interface, weakening the interfacial bonding and possible cathodic delamination of the coating from the mild steel substrates.[57] The highest wet adhesion strength was observed for EP-DCS-10 samples. The increment of the wet adhesion strength in the presence of Ep-DCS and Am-DCS compared to EP and EP-CHS-2 coatings can be related to the barrier properties of the carbon capsules restricting the diffusion of electrolyte through the epoxy matrix to the metal/coating interface. As a consequence, the addition of Ep-DCSs and Am-DCSs in the epoxy coating reduced the adhesion loss demonstrated by the lowest adhesion loss for the EP-DCS-10 sample as shown in Figure 6b.

The dry adhesion of epoxy coatings was enhanced in the presence of doped carbon capsules compared to EP sample presumably due to the chemical interactions between NH_2 groups grafted on the surface of carbon capsules, epoxide groups of epoxy chains, and hydroxyl groups of steel surface. Nonetheless, in the presence of 5 and 10 wt % Ep-DCSs, the dry adhesion strength of EP-DCS-5 and EP-DCS-10 samples is lower than that of EP-DCS-2. It seems that the molecular interactions and adhesion mechanisms between epoxy chains, carbon spheres, and the steel surface are affected by the doped carbon capsule loading in the coatings.

3.4. ATR-FTIR. As presented in section 3.3, the dry adhesion strength of EP-DCS-5 and EP-DCS-10 samples decreased with incorporation of the doped carbon capsules in comparison with EP and EP-DCS-2 coatings. The interaction modes between epoxy chains, doped carbon capsules, and the steel substrate were evaluated in situ employing ATR-FTIR in a Kretschmann geometry. For this purpose, uncured EP and EP-DCS-10 coatings containing the curing agents were applied on the surface of IREs coated with a thin layer of pure iron and the ATR-FTIR spectra of the samples during the curing process of the coatings were recorded upon casting of the liquid coatings on the IREs. It is worth mentioning that the metal and polymer interfaces are analyzed using Ge, while bulk polymer functional groups are investigated by ZnSe as an IRE having a lower reflection index.[58−60] Figure 7 schematically presents the respective probing regions by Ge and ZnSe IREs.

The ATR-FTIR spectra of fully cured EP and EP-DCS-10 samples and their corresponding characteristic peaks detected by Ge and ZnSe IREs are shown in Figure 7. As shown, there is no difference between ATR-FTIR spectra and their related characteristic peaks of the EP sample detected by Ge and ZnSe IREs. The wide peak at ∼3390 cm^{-1} is linked to the stretching vibration of O−H bonds of hydroxyl groups in the cross-linked epoxy−polyamine networks. The absorbance peaks related to CH_3 and CH_2 groups as well as C−H stretching of oxirane rings are located at ∼2912, ∼2860, and ∼732 cm^{-1}, respectively. The corresponding peak of N−H bond related to polyamine groups appeared at ∼1720 cm^{-1}. The peaks of C−C (∼1604 cm^{-1}), C═C (∼1508 cm^{-1}), C−O (∼1241 cm^{-1}), and C−O−C (∼1033 and ∼828 cm^{-1}) are assigned to the backbones of the epoxy chains.

The main characteristic peaks of the EP-DCS-10 sample detected by the ZnSe IRE are similar to those of PE coating probed by Ge and ZnSe IREs. However, some new peaks can be seen in the ATR-FTIR spectrum of EP-DCS-10 detected by Ge IRE indicating the different interactions with the iron surface

DOI: 10.1021/acs.iecr.8b06306
Ind. Eng. Chem. Res. 2019, 58, 3033−3046

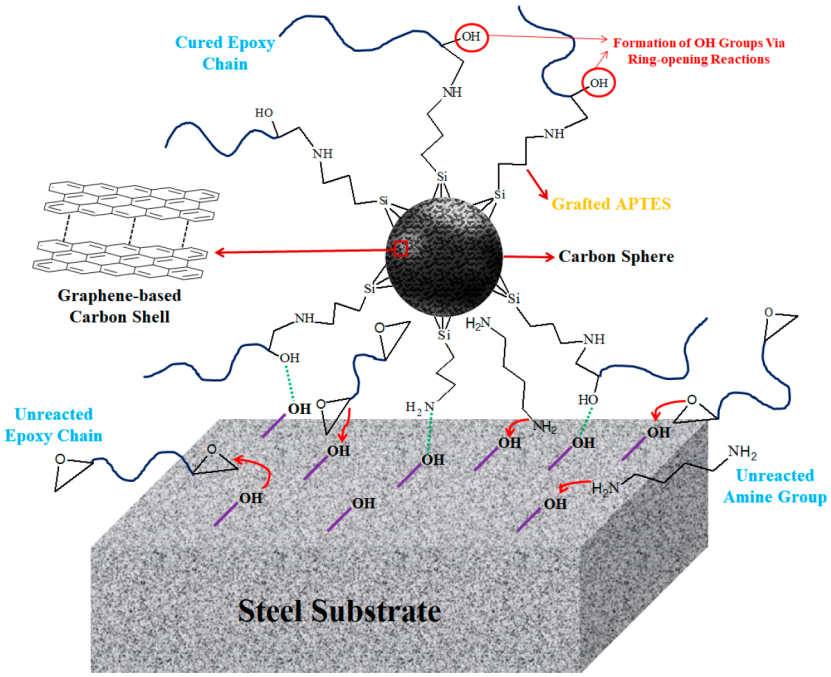

Figure 8. Schematic illustration of chemical interactions between NH_2 groups of APTES grafted on the surface of carbon capsules, cured and uncured epoxy and polyamine groups, and hydroxyl groups of the steel surface.

compared to the EP sample. The lower intensity of all peaks and appearance of new peaks related to the unreacted epoxide groups (~894 and ~933 cm^{-1}) and overlapped Si−O−C with C−O−C bonds (~1085 cm^{-1}) demonstrate the presence of some carbon capsules at the interface with the iron substrate. Si−O−C and C−O−C bonds are attributed to APTES grafted on the surface of carbon capsules and unreacted epoxy groups released from Ep-DCSs at the metal/polymer interface. Near the metal surface, the released epoxy and polyamine chains have no chain mobility to react effectively with each other. It can be deduced from these observations that the contact surface of the epoxy matrix with the iron decreases and the stoichiometry ratio of epoxy and polyamine groups near the metal/polymer interface changes leading to the lower dry adhesion strength of EP-DCS-5 and EP-DCS-10 samples.

Also, the lower intensity of the O−H bond peak shown in the spectra of EP-DCS-10 probed by Ge IRE compared to that by the ZnSe one can be related to fewer reactions between epoxy and polyamine in the metal/polymer interface because of the lower chain mobility near the metal surface resulting in lower formation of hydroxyl groups in the cross-linked epoxy−polyamine networks produced via ring-opening reactions of epoxide groups (see Figure 8). Thus, the cross-linking density at the metal/polymer interface seems to be lower for EP-DCS-5 and EP-DCS-10 samples compared to EP-DCS-2. Figure 8 schematically presents the possible chemical interactions between NH_2 groups of APTES grafted on the surface of carbon capsules, cured and uncured epoxy and polyamine groups and hydroxyl groups of the steel surface.

3.6. Corrosion Protection by the Nanocomposite Coatings. EIS measurements were performed to investigate the effect of epoxy/polyamine dual-encapsulated carbon capsules on the corrosion protection performance of the epoxy coatings at different immersion times in 3.5 wt % NaCl solution. The Nyquist and Bode plots of the blank epoxy and nanocomposite coatings are illustrated in Figure 9. The corrosion protection performance of the coatings can be compared by the values of total impedance at low frequency ($|Z|_{0.01\ Hz}$) which, at constant electrolyte resistance values, is indicative of the coating's polarization and interfacial charge transfer resistance of the coated sample.[61] Figure 9 indicates that after 5 days immersion in the corrosive solution, $|Z|_{0.01\ Hz}$ values for all samples are higher than $10^8\ \Omega\ cm^2$, and values of the phase angle are about −90°. EP-DCS-10 coating showed capacitive behavior in a wide frequency range while other coatings present capacitive behavior in the frequency range of 1 Hz to 10 kHz. This shows a partial diffusion of the electrolyte through these coatings after 5 days exposure in the corrosive solution. For all coatings, after 5 days immersion, the one-time constant behavior can be observed in EIS plots indicating a limited decrement of barrier properties for all coatings. However, a two-time constant electrochemical impedance behavior can be observed in Nyquist and Bode plots of EP sample after 5 days and EP-DCS-2 and EP-DCS-5 samples after 25 days of immersion. Coatings barrier properties declined with increasing immersion time due to electrolyte diffusion through the epoxy coatings. Figure 9b shows the Bode plot of EP-DCS-10 coating after 5 days exposure to the corrosive electrolyte with a straight line of −1 slope indicating an intact coating/metal interface. An indication of coating degradation with immersion time is the reduction of the frequency range in which the capacitive behavior is dominant, resulting in the decrease of the impedance modulus and barrier properties of the coatings. Creation of electrolyte pathways toward the steel substrates resulted in broadening of the resistive behavior (in the low-frequency region) of the coatings, indicating deterioration of the protective coating properties.

The values of the impedance modulus at low frequency ($|Z|_{0.01\ Hz}$) and breakpoint frequency (f_b) of the different coatings during immersion time are illustrated in Figure 10. f_b is defined the frequency in which the phase angle is equal to −45°.

As shown, $|Z|_{0.01\ Hz}$ of all coatings at early immersion times (5 days) is high, indicating good barrier and corrosion protective

DOI: 10.1021/acs.iecr.8b06306
Ind. Eng. Chem. Res. 2019, 58, 3033−3046

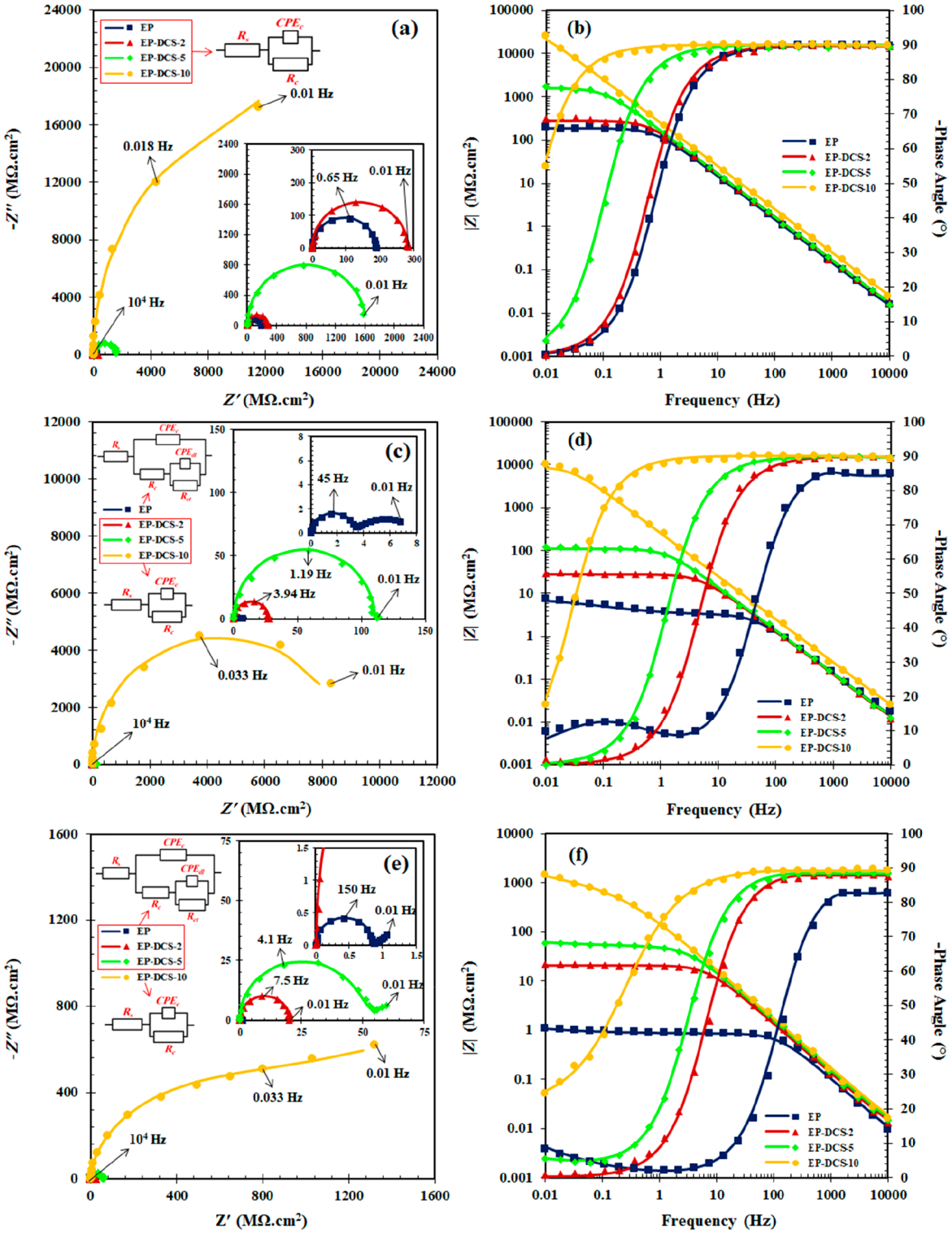

Figure 9. Nyquist (a, c, and e) and Bode (b, d, and f) plots of the blank epoxy and nanocomposite coatings immersed for 5 (a and b), 25 (c and d), and 50 days (e and f) in 3.5 wt % NaCl solution. The fitted and experimental data are presented by solid lines and markers, respectively.

properties of the coatings. Also, the higher low-frequency impedance and related corrosion protection were observed for the coatings containing a higher concentration of the doped carbon capsules.

The low-frequency impedance decreases with immersion time due to the degradation of the coatings by the exposure to the saline solution. The corrosion protection performance of the coatings can also be determined from Bode plots by the value of f_b. The f_b for the coatings is related to the corrosion protectiveness and disbonded area.[2,4] According to Figure 10b, the epoxy coatings containing higher contents of doped carbon capsules show a lower f_b. Also, f_b of all coatings is shifted to higher frequencies with immersion time. This phenomenon is the most pronounced for EP revealing a decrease of the capacitive behavior due to the electrolyte diffusion into the coatings.

DOI: 10.1021/acs.iecr.8b06306
Ind. Eng. Chem. Res. 2019, 58, 3033−3046

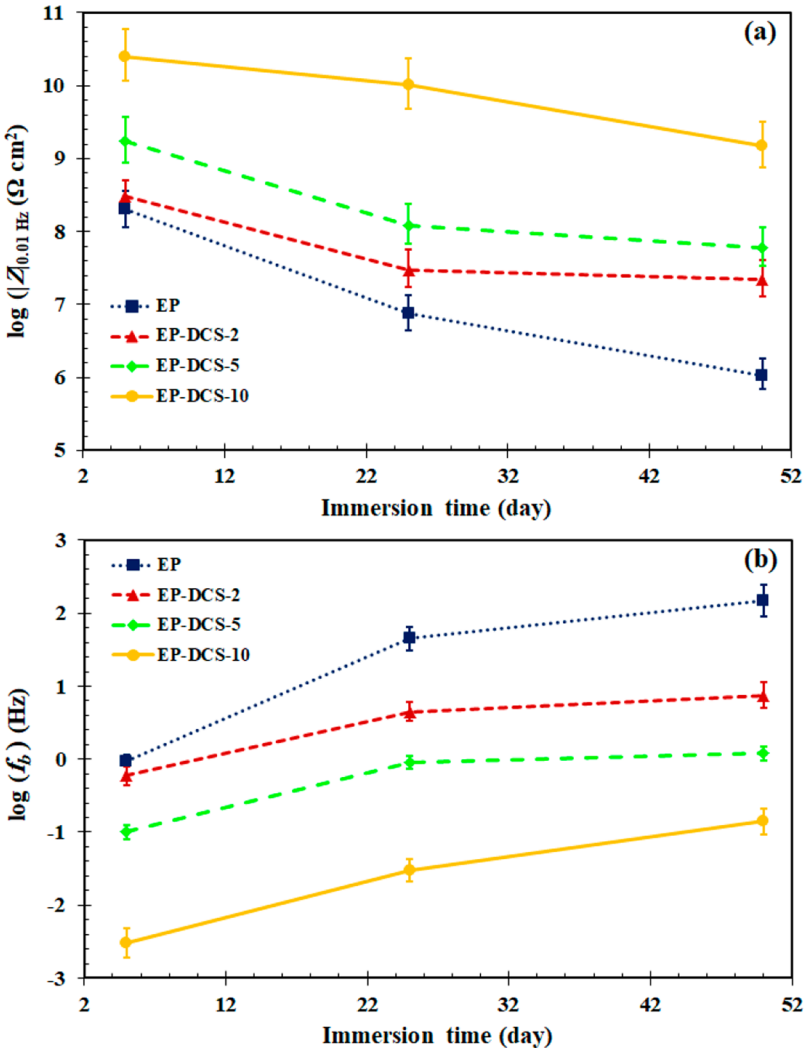

Figure 10. Values of the impedance at low frequency (a) and breakpoint frequency (b) of the different coatings immersed in 3.5 wt % NaCl solution as a function of immersion time.

The frequencies of the intersection points of Bode impedance and Bode phase angle plots have also been reported to be related to the barrier and corrosion protection performance of the coatings.[2,62] Degradation of coatings due to the electrolyte uptake leads to the shifting of the frequency of intersection point of impedance and phase angle plots to the higher frequencies.[2] The variations in intersection Bode plots (IBP) of all coatings versus the immersion times are presented in Figure 11. With immersion time, IBP values of all samples are shifted to higher frequencies indicating that the corrosive electrolyte continuously diffuses into the coatings. Also, EP has a higher IBP value compared to the nanocomposite coatings. It is inferred that the addition of Ep-DCSs and Am-DCSs in the epoxy matrix decreases the diffusion rate of the corrosive electrolyte into the coating leading to a shift of IBP and f_b values to the lower frequencies.

To model the EIS data, one-time and two-time constant electrical equivalent circuits were used as illustrated in Figure 9. As shown in these models, Solution resistance (R_s), coating resistance (R_c), constant phase element of coating (CPE_c), constant phase element of double layer (CPE_{dl}), and charge transfer resistance (R_{ct}) were used to model the EIS spectra. The coating capacitance (C_c) values were calculated using eq 4:[63]

$$C_c = \frac{(R_c Y_0)^{1/n}}{R_c} \quad (4)$$

in which Y_0 and n are CPE admittance and exponent, respectively. The calculated R_c and C_c values are shown in Figure 12. As shown in Figure 12a, the addition of doped carbon capsules in the epoxy coating significantly increased R_c of the nanocomposite coatings. Also, all coatings experienced a descending trend for R_c with immersion time as a result of the electrolyte diffusion through the coating and formation of corrosion products under the coatings.

Inclusion of the carbon capsules in microcavities and pores of the epoxy matrix blocked the electrolyte pathways in the coating and postponed the coating deterioration as shown schematically in Figure 13a. A close relationship can be found between the diffusion behavior of the electrolyte in the coating and the coating capacitance.[2,9] The coating with low capacitance is less permeable than those with the higher capacitance. It can be observed from Figure 12b that C_c values for the coatings with the higher contents of Ep-DCSs and Am-DCSs are much lower compared to the others. The increment of C_c with the immersion time is related to the water uptake of the epoxy coatings. All these observations indicate that epoxy coatings

DOI: 10.1021/acs.iecr.8b06306
Ind. Eng. Chem. Res. 2019, 58, 3033−3046

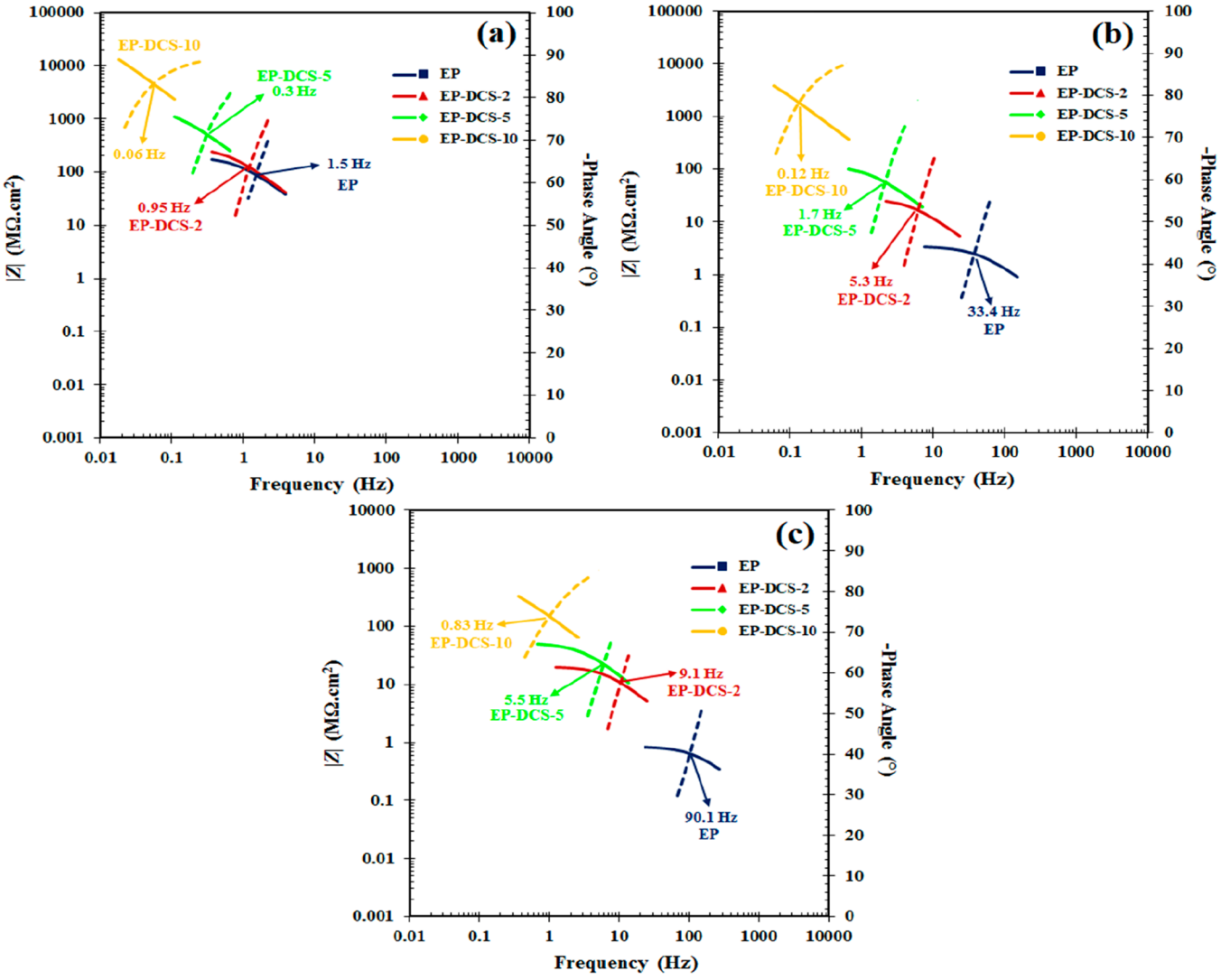

Figure 11. IBP values of the different coatings immersed for 5 (a), 25, (b) and 50 days (c) in 3.5 wt % NaCl solution.

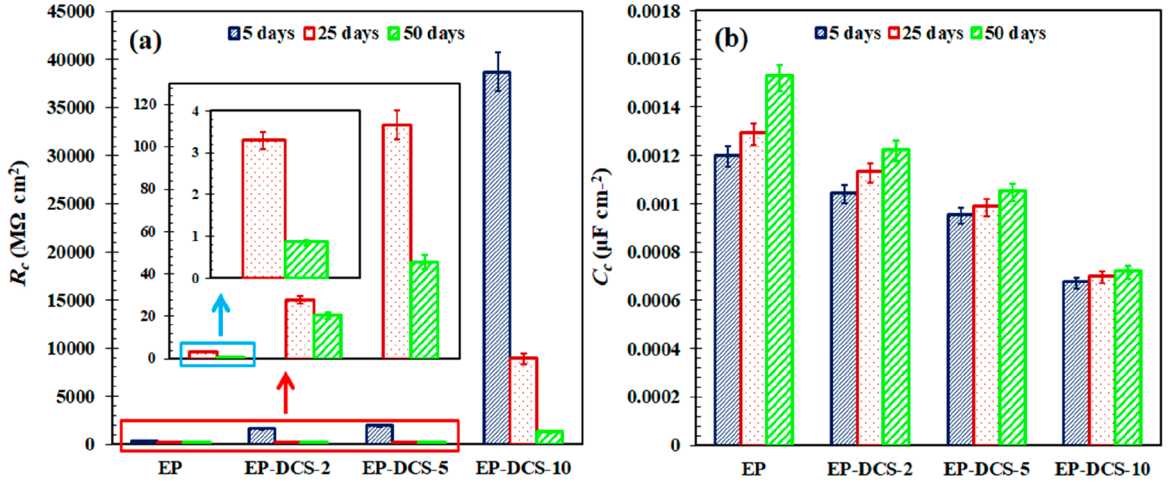

Figure 12. Values of R_c (a) and C_c (b) of the coatings immersed for different immersion times in 3.5 wt % NaCl solution obtained from the fitted data.

containing higher concentrations of carbon capsules demonstrate the better corrosion protection properties and higher barrier properties against the aggressive components as shown in Figure 13. Three main reasons can be provided for the better corrosion protection properties of the epoxy coating containing the doped carbon capsules. First, the addition of impermeable carbon capsules reduces the diffusion rate and increases the diffusion length of the corrosive electrolyte into the coating. Moreover, S_N2-type nucleophilic substitution ring-opening reactions can take place between grafted NH_2 groups on the

DOI: 10.1021/acs.iecr.8b06306
Ind. Eng. Chem. Res. 2019, 58, 3033−3046

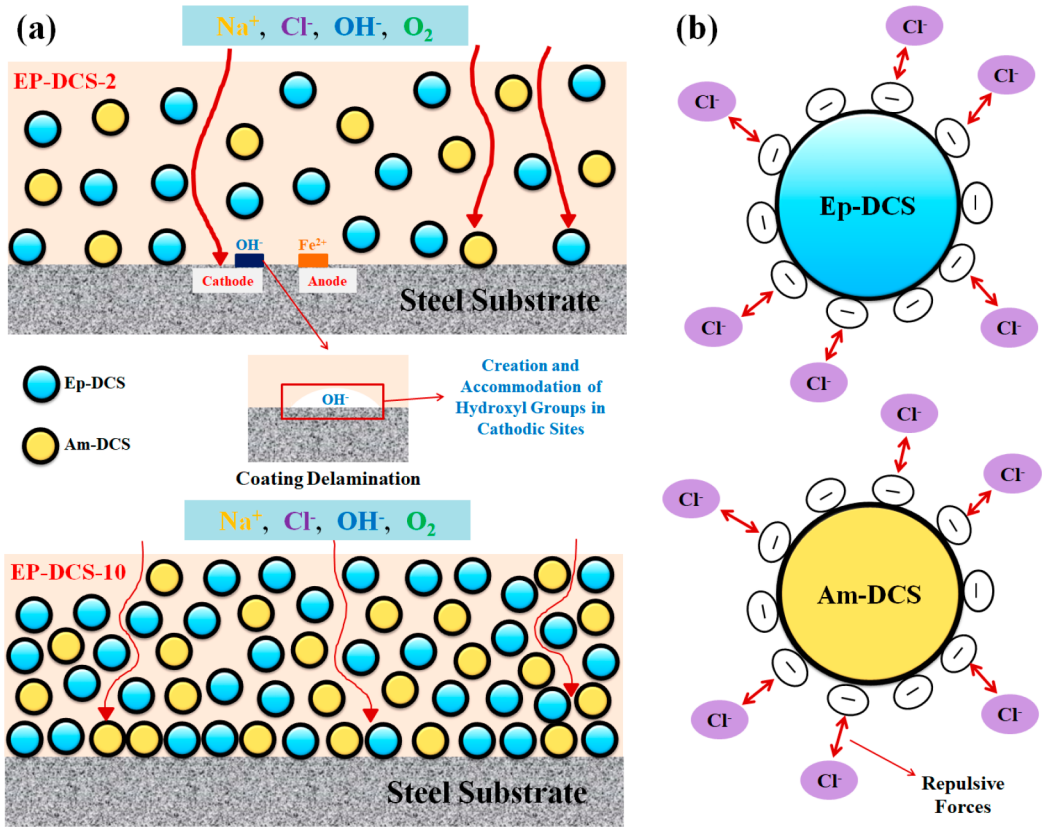

Figure 13. Schematic illustration of the barrier and corrosion protection performance of epoxy coatings containing various contents of doped carbon capsules (a) and formation of repulsive forces between carbon capsules with chloride ions (b).

surface of carbon capsules and epoxide groups of the epoxy chains increasing the cross-linking density of the epoxy matrix around carbon capsules (see Figure 13) and barrier properties of nanocomposite coatings.[4] As we reported in our previous publication,[36] ζ potential measurements showed that carbon capsules have a negative surface charge at pHs higher than 7. Dispersion of carbon capsules with a negative charge in the epoxy matrix resist the transport of Cl^- and other aggressive ions with a negative charge through the coating because of the repulsive forces shown schematically in Figure 13b. Furthermore, gradual release of epoxy and polyamine film-forming agents from Ep-DCSs and Am-DCSs to structural defects, micropores, and cavities of the epoxy coating and partial reactions between them may be another reason for better corrosion performance of carbon capsule loaded epoxy coatings.

4. CONCLUSIONS

The effects of epoxy/polyamine dual-encapsulated carbon capsules at different concentrations on the mechanical and corrosion protection properties of the nanocomposite epoxy coating were studied. It was shown that incorporation of doped carbon capsules in the epoxy matrix notably enhanced its barrier properties and corrosion protection performance. Tensile test results showed that mechanical properties including tensile strength, Young's modulus, and toughness of the epoxy coatings increased in the presence of carbon capsules. Also, the epoxy coatings with higher concentrations of carbon capsules showed higher scratch hardness. EIS and pull-off results revealed that the corrosion resistance and wet adhesion strength of nanocomposite coatings increased with increasing doped carbon capsules concentrations. Also, adhesion loss of nanocomposite coatings decreased due to the good barrier properties of epoxy coatings in the presence of carbon nanospheres. NH_2 groups grafted on the carbon capsules provided proper interactions with the epoxy chains leading to a uniform distribution in the epoxy matrix. Furthermore, chemical interactions between NH_2 groups of carbon capsules, epoxy chains, and the steel substrate surface were found to be responsible for the enhanced mechanical and corrosion protective properties.

AUTHOR INFORMATION

Corresponding Author

*E-mail: ramazani@sharif.edu.

ORCID

A. Ramazani S. A.: 0000-0002-0095-6104
M. Mahdavian: 0000-0001-8470-6833
J. M. C. Mol: 0000-0003-1810-5145

Notes

The authors declare no competing financial interest.

REFERENCES

(1) Behzadnasab, M.; Mirabedini, S. M.; Esfandeh, M. Corrosion Protection of Steel by Epoxy Nanocomposite Coatings Containing Various Combinations of Clay and Nanoparticulate Zirconia. *Corros. Sci.* **2013**, *75*, 134−141.

(2) Ramezanzadeh, B.; Ghasemi, E.; Mahdavian, M.; Changizi, E.; Mohamadzadeh Moghadam, M. H. Covalently-Grafted Graphene Oxide Nanosheets to Improve Barrier and Corrosion Protection Properties of Polyurethane Coatings. *Carbon* **2015**, *93*, 555−573.

(3) Maksimović, M. D.; Mišković-Stanković, V. B. The Corrosion Behaviour of Epoxy-Resin Electrocoated Steel. *Corros. Sci.* **1992**, *33* (2), 271−279.

DOI: 10.1021/acs.iecr.8b06306
Ind. Eng. Chem. Res. 2019, 58, 3033−3046

(4) Ramezanzadeh, B.; Niroumandrad, S.; Ahmadi, A.; Mahdavian, M.; Moghadam, M. H. M. Enhancement of Barrier and Corrosion Protection Performance of an Epoxy Coating through Wet Transfer of Amino Functionalized Graphene Oxide. *Corros. Sci.* **2016**, *103*, 283−304.
(5) Mahdavian, M.; Naderi, R.; Peighambari, M.; Hamdipour, M.; Haddadi, S. A. Evaluation of Cathodic Disbondment of Epoxy Coating Containing Azole Compounds. *J. Ind. Eng. Chem.* **2015**, *21*, 1167−1173.
(6) May, C. A. Introduction to Epoxy Resins. *Epoxy Resins*, 2nd ed.; Routledge, 2018; pp 15−22.
(7) Pizzi, A.; Mittal, K. L. *Handbook of Adhesive Technology*, 3rd ed.; CRC Press, 2017.
(8) Lee, H.; Neville, K. Book Review-Handbook of Epoxy Resins. *Ind. Eng. Chem.* **1967**, *59* (9), 16−17.
(9) Ramezanzadeh, B.; Haeri, Z.; Ramezanzadeh, M. A Facile Route of Making Silica Nanoparticles-Covered Graphene Oxide Nanohybrids (SiO2-GO); Fabrication of SiO2-GO/Epoxy Composite Coating with Superior Barrier and Corrosion Protection Performance. *Chem. Eng. J.* **2016**, *303*, 511−528.
(10) Meng, F.; Liu, L.; Tian, W.; Wu, H.; Li, Y.; Zhang, T.; Wang, F. The Influence of the Chemically Bonded Interface between Fillers and Binder on the Failure Behaviour of an Epoxy Coating under Marine Alternating Hydrostatic Pressure. *Corros. Sci.* **2015**, *101*, 139−154.
(11) Chruściel, J. J.; Leśniak, E. Modification of Epoxy Resins with Functional Silanes, Polysiloxanes, Silsesquioxanes, Silica and Silicates. *Prog. Polym. Sci.* **2015**, *41*, 67−121.
(12) Jiang, M.-Y.; Wu, L.-K.; Hu, J.-M.; Zhang, J.-Q. Silane-Incorporated Epoxy Coatings on Aluminum Alloy (AA2024). Part 2: Improved Corrosion Performance. *Corros. Sci.* **2015**, *92*, 127−135.
(13) Jiang, M.-Y.; Wu, L.-K.; Hu, J.-M.; Zhang, J.-Q. Silane-Incorporated Epoxy Coatings on Aluminum Alloy (AA2024). Part 1: Improved Corrosion Performance. *Corros. Sci.* **2015**, *92*, 118−126.
(14) Alizadeh Razin, A.; Ramezanzadeh, B.; Yari, H. Detecting and Estimating the Extent of Automotive Coating Delamination and Damage Indexes after Stone Chipping Using Electrochemical Impedance Spectroscopy. *Prog. Org. Coat.* **2016**, *92*, 95−109.
(15) Zheludkevich, M. L.; Poznyak, S. K.; Rodrigues, L. M.; Raps, D.; Hack, T.; Dick, L. F.; Nunes, T.; Ferreira, M. G. S. Active Protection Coatings with Layered Double Hydroxide Nanocontainers of Corrosion Inhibitor. *Corros. Sci.* **2010**, *52* (2), 602−611.
(16) MengQiu, M. Y. J. Application of Glass Flakes in Novolac-Epoxy Vinyl Ester Resin Anticorrosive Coatings [J]. *J. Beijing Univ. Chem. Technol., Nat. Sci. Ed.* **2007**, *2*, 9.
(17) Ramezanzadeh, B.; Arman, S. Y.; Mehdipour, M. Anticorrosion Properties of an Epoxy Zinc-Rich Composite Coating Reinforced with Zinc, Aluminum, and Iron Oxide Pigments. *J. Coatings Technol. Res.* **2014**, *11* (5), 727−737.
(18) Liu, Z. M.; Miao, Q.; Liang, W. P.; Jiang, Q.; Wang, K. Effect of Aluminum Content in Zinc-Aluminum Alloy Powder on Anticorrosion Behavior of Chromium-Free Dacromet Coating. *Mater. Prot.* **2015**, *48* (3), 16.
(19) Askari, F.; Ghasemi, E.; Ramezanzadeh, B.; Mahdavian, M. Mechanistic Approach for Evaluation of the Corrosion Inhibition of Potassium Zinc Phosphate Pigment on the Steel Surface: Application of Surface Analysis and Electrochemical Techniques. *Dyes Pigm.* **2014**, *109*, 189−199.
(20) Alibakhshi, E.; Ghasemi, E.; Mahdavian, M. Optimization of Potassium Zinc Phosphate Anticorrosion Pigment by Taguchi Experimental Design. *Prog. Org. Coat.* **2013**, *76* (1), 224−230.
(21) Alibakhshi, E.; Naeimi, A.; Ramezanzadeh, M.; Ramezanzadeh, B.; Mahdavian, M. A Facile Synthesis Method of an Effective Anti-Corrosion Nanopigment Based on Zinc Polyphosphate through Microwaves Assisted Combustion Method; Comparing the Influence of Nanopigment and Conventional Zinc Phosphate on the Anti-Corrosion Properties of an E. *J. Alloys Compd.* **2018**, *762*, 730−744.
(22) Haddadi, S. A.; Mahdavian, M.; Karimi, E. Evaluation of the Corrosion Protection Properties of an Epoxy Coating Containing Sol−gel Surface Modified Nano-Zirconia on Mild Steel. *RSC Adv.* **2015**, *5* (36), 28769−28777.
(23) Ghazizadeh, A.; Haddadi, S. A.; Mahdavian, M. The Effect of Sol−gel Surface Modified Silver Nanoparticles on the Protective Properties of the Epoxy Coating. *RSC Adv.* **2016**, *6* (23), 18996−19006.
(24) Peres, R. N.; Cardoso, E. S. F.; Montemor, M. F.; De Melo, H. G.; Benedetti, A. V.; Suegama, P. H. Influence of the Addition of SiO2 Nanoparticles to a Hybrid Coating Applied on an AZ31 Alloy for Early Corrosion Protection. *Surf. Coat. Technol.* **2016**, *303*, 372−384.
(25) Sharifi Golru, S.; Attar, M. M.; Ramezanzadeh, B. Studying the Influence of Nano-Al2O3 Particles on the Corrosion Performance and Hydrolytic Degradation Resistance of an Epoxy/Polyamide Coating on AA1050. *Prog. Org. Coat.* **2014**, *77* (9), 1391−1399.
(26) Ghaffari, M.; Ehsani, M.; Vandalvand, M.; Avazverdi, E.; Askari, A.; Goudarzi, A. Studying the Effect of Micro-and Nano-Sized ZnO Particles on the Curing Kinetic of Epoxy/Polyaminoamide System. *Prog. Org. Coat.* **2015**, *89*, 277−283.
(27) Palimi, M. J.; Rostami, M.; Mahdavian, M.; Ramezanzadeh, B. A Study on the Corrosion Inhibition Properties of Silane-Modified Fe2O3 Nanoparticle on Mild Steel and Its Effect on the Anticorrosion Properties of the Polyurethane Coating. *J. Coatings Technol. Res.* **2015**, *12* (2), 277−292.
(28) Palimi, M. J.; Rostami, M.; Mahdavian, M.; Ramezanzadeh, B. Application of EIS and Salt Spray Tests for Investigation of the Anticorrosion Properties of Polyurethane-Based Nanocomposites Containing Cr2O3 Nanoparticles Modified with 3-Amino Propyl Trimethoxy Silane. *Prog. Org. Coat.* **2014**, *77* (11), 1935−1945.
(29) Deyab, M. A.; Nada, A. A.; Hamdy, A. Comparative Study on the Corrosion and Mechanical Properties of Nano-Composite Coatings Incorporated with TiO2 Nano-Particles, TiO2 Nano-Tubes, and ZnO Nano-Flowers. *Prog. Org. Coat.* **2017**, *105*, 245−251.
(30) Lewis, O. D.; Critchlow, G. W.; Wilcox, G. D.; deZeeuw, A.; Sander, J. A Study of the Corrosion Resistance of a Waterborne Acrylic Coating Modified with Nano-Sized Titanium Dioxide. *Prog. Org. Coat.* **2012**, *73* (1), 88−94.
(31) Wang, C.; Bai, Y.; Bai, Y.; Gao, J.; Ma, W. Enhancement of Corrosion Resistance and Bioactivity of Titanium by Au Nanoparticle-Loaded TiO2 Nanotube Layer. *Surf. Coat. Technol.* **2016**, *286*, 327−334.
(32) Hang, T. T. X.; Truc, T. A.; Olivier, M.-G.; Vandermiers, C.; Guérit, N.; Pébère, N. Corrosion Protection Mechanisms of Carbon Steel by an Epoxy Resin Containing Indole-3 Butyric Acid Modified Clay. *Prog. Org. Coat.* **2010**, *69* (4), 410−416.
(33) Almajid, A.; Sorochynska, L.; Friedrich, K.; Wetzel, B. Effects of Graphene and CNT on Mechanical, Thermal, Electrical and Corrosion Properties of Vinylester Based Nanocomposites. *Plast., Rubber Compos.* **2015**, *44* (2), 50−62.
(34) Khamseh, S.; Alibakhshi, E.; Mahdavian, M.; Saeb, M. R.; Vahabi, H.; Kokanyan, N.; Laheurte, P. Magnetron-Sputtered Copper/Diamond-like Carbon Composite Thin Films with Super Anti-Corrosion Properties. *Surf. Coat. Technol.* **2018**, *333*, 148−157.
(35) Liu, D.; Zhao, W.; Liu, S.; Cen, Q.; Xue, Q. Comparative Tribological and Corrosion Resistance Properties of Epoxy Composite Coatings Reinforced with Functionalized Fullerene C60 and Graphene. *Surf. Coat. Technol.* **2016**, *286*, 354−364.
(36) Haddadi, S. A.; Ramazani, S. A. A.; Mahdavian, M.; Taheri, P.; Mol, J. M. C. Fabrication and Characterization of Graphene-Based Carbon Hollow Spheres for Encapsulation of Organic Corrosion Inhibitors. *Chem. Eng. J.* **2018**, *352* (June), 909−922.
(37) Pirhady Tavandashti, N.; Ghorbani, M.; Shojaei, A.; Mol, J. M. C.; Terryn, H.; Baert, K.; Gonzalez-Garcia, Y. Inhibitor-Loaded Conducting Polymer Capsules for Active Corrosion Protection of Coating Defects. *Corros. Sci.* **2016**, *112*, 138−149.
(38) García, S. J.; Fischer, H. R.; White, P. A.; Mardel, J.; González-García, Y.; Mol, J. M. C.; Hughes, A. E. Self-Healing Anticorrosive Organic Coating Based on an Encapsulated Water Reactive Silyl Ester: Synthesis and Proof of Concept. *Prog. Org. Coat.* **2011**, *70* (2), 142−149.

DOI: 10.1021/acs.iecr.8b06306
Ind. Eng. Chem. Res. 2019, 58, 3033−3046

(39) Alibakhshi, E.; Ghasemi, E.; Mahdavian, M.; Ramezanzadeh, B. A Comparative Study on Corrosion Inhibitive Effect of Nitrate and Phosphate Intercalated Zn-Al- Layered Double Hydroxides (LDHs) Nanocontainers Incorporated into a Hybrid Silane Layer and Their Effect on Cathodic Delamination of Epoxy Topcoat. *Corros. Sci.* **2017**, *115*, 159−174.
(40) Abdullayev, E.; Price, R.; Shchukin, D.; Lvov, Y. Halloysite Tubes as Nanocontainers for Anticorrosion Coating with Benzotriazole. *ACS Appl. Mater. Interfaces* **2009**, *1* (7), 1437−1443.
(41) Ghazi, A.; Ghasemi, E.; Mahdavian, M.; Ramezanzadeh, B.; Rostami, M. The Application of Benzimidazole and Zinc Cations Intercalated Sodium Montmorillonite as Smart Ion Exchange Inhibiting Pigments in the Epoxy Ester Coating. *Corros. Sci.* **2015**, *94*, 207−217.
(42) Wei, H.; Wang, Y.; Guo, J.; Shen, N. Z.; Jiang, D.; Zhang, X.; Yan, X.; Zhu, J.; Wang, Q.; Shao, L.; Lin, H.; Wei, S.; Guo, Z. Advanced Micro/Nanocapsules for Self-Healing Smart Anticorrosion Coatings. *J. Mater. Chem. A* **2015**, *3* (2), 469−480.
(43) Dias, S. A. S.; Lamaka, S. V.; Nogueira, C. A.; Diamantino, T. C.; Ferreira, M. G. S. Sol−gel Coatings Modified with Zeolite Fillers for Active Corrosion Protection of AA2024. *Corros. Sci.* **2012**, *62*, 153−162.
(44) Andreeva, D. V.; Skorb, E. V. Multi-Layer Smart Coatings for Corrosion Protection of Aluminium Alloys and Steel. *Handb. Smart Coatings Mater. Prot.* **2014**, 307−327.
(45) Siva, T.; Sathiyanarayanan, S. Self Healing Coatings Containing Dual Active Agent Loaded Urea Formaldehyde (UF) Microcapsules. *Prog. Org. Coat.* **2015**, *82*, 57−67.
(46) Yi, H.; Deng, Y.; Wang, C. Pickering Emulsion-Based Fabrication of Epoxy and Amine Microcapsules for Dual Core Self-Healing Coating. *Compos. Sci. Technol.* **2016**, *133*, 51−59.
(47) Jin, H.; Mangun, C. L.; Stradley, D. S.; Moore, J. S.; Sottos, N. R.; White, S. R. Self-Healing Thermoset Using Encapsulated Epoxy-Amine Healing Chemistry. *Polymer* **2012**, *53* (2), 581−587.
(48) Leal, D. A.; Riegel-Vidotti, I. C.; Ferreira, M. G. S.; Marino, C. E. B. Smart Coating Based on Double Stimuli-Responsive Microcapsules Containing Linseed Oil and Benzotriazole for Active Corrosion Protection. *Corros. Sci.* **2018**, *130*, 56−63.
(49) Zhang, H.; Wang, J.; Liu, X.; Wang, Z.; Wang, S. High Performance Self-Healing Epoxy/Polyamide Protective Coating Containing Epoxy Microcapsules and Polyaniline Nano Fi Bers for Mild Carbon Steel. *Ind. Eng. Chem. Res.* **2013**, *52*, 10172−10180.
(50) Briscoe, B. J.; Pelillo, E.; Sinha, S. K. Scratch Hardness and Deformation Maps for Polycarbonate and Polyethylene. *Polym. Eng. Sci.* **1996**, *36* (24), 2996−3005.
(51) Haddadi, S. A.; Ramazani S. A., A.; Amini, M.; Kheradmand, A. In-Situ Preparation and Characterization of Ultra-High Molecular Weight Polyethylene/Diamond Nanocomposites Using Bi-Supported Ziegler-Natta Catalyst: Effect of Nanodiamond Silanization. *Mater. Today Commun.* **2018**, *14*, 53−64.
(52) Haddadi, S. A.; Ramazani S. A., A.; Talebi, S.; Fattahpour, S.; Hasany, M. Investigation of the Effect of Nanosilica on Rheological, Thermal, Mechanical, Structural, and Piezoelectric Properties of PVDF Nanofibers Fabricated Using Electrospinning Technique. *Ind. Eng. Chem. Res.* **2017**, *56*, 12596−12607.
(53) Palimi, M. J.; Rostami, M.; Mahdavian, M.; Ramezanzadeh, B. Surface Modification of Cr2O3 Nanoparticles with 3-Amino Propyl Trimethoxy Silane (APTMS). Part 1: Studying the Mechanical Properties of Polyurethane/Cr2O3 Nanocomposites. *Prog. Org. Coat.* **2014**, *77* (11), 1663−1673.
(54) Palimi, M. J.; Rostami, M.; Mahdavian, M.; Ramezanzadeh, B. Surface Modification of Fe2O3 Nanoparticles with 3-Aminopropyl-trimethoxysilane (APTMS): An Attempt to Investigate Surface Treatment on Surface Chemistry and Mechanical Properties of Polyurethane/Fe2O3 Nanocomposites. *Appl. Surf. Sci.* **2014**, *320*, 60−72.
(55) Sun, Y.; Zhang, Z.; Wong, C. P. Study on Mono-Dispersed Nano-Size Silica by Surface Modification for Underfill Applications. *J. Colloid Interface Sci.* **2005**, *292* (2), 436−444.
(56) Papageorgiou, D. G.; Kinloch, I. A.; Young, R. J. Mechanical Properties of Graphene and Graphene-Based Nanocomposites. *Prog. Mater. Sci.* **2017**, *90*, 75−127.
(57) Ramezanzadeh, B.; Raeisi, E.; Mahdavian, M. Studying Various Mixtures of 3-Aminopropyltriethoxysilane (APS) and Tetraethylorthosilicate (TEOS) Silanes on the Corrosion Resistance of Mild Steel and Adhesion Properties of Epoxy Coating. *Int. J. Adhes. Adhes.* **2015**, *63*, 166−176.
(58) Taheri, P.; Flores, J. R.; Hannour, F.; De Wit, J. H. W.; Terryn, H.; Mol, J. M. C. In Situ Study of Buried Interfacial Bonding Mechanisms of Carboxylic Polymers on Zn Surfaces. *J. Phys. Chem. C* **2013**, *117* (7), 3374−3382.
(59) Sababi, M.; Terryn, H.; Mol, J. M. C. The Influence of a Zr-Based Conversion Treatment on Interfacial Bonding Strength and Stability of Epoxy Coated Carbon Steel. *Prog. Org. Coat.* **2017**, *105*, 29−36.
(60) Taheri, P.; De Wit, J. H. W.; Terryn, H.; Mol, J. M. C. In Situ Study of Buried Metal−Polymer Interfaces Exposed to an Aqueous Solution by an Integrated ATR-FTIR and Electrochemical Impedance Spectroscopy System. *J. Phys. Chem. C* **2013**, *117* (40), 20826−20832.
(61) Mahdavian, M.; Attar, M. M. Another Approach in Analysis of Paint Coatings with EIS Measurement: Phase Angle at High Frequencies. *Corros. Sci.* **2006**, *48* (12), 4152−4157.
(62) Xu, A.; Zhang, F.; Jin, F.; Zhang, R.; Luo, B.; Zhang, T. The Evaluation of Coating Performance by Analyzing the Intersection of Bode Plots. *Int. J. Electrochem. Sci.* **2014**, *9*, 5116−5125.
(63) Hirschorn, B.; Orazem, M. E.; Tribollet, B.; Vivier, V.; Frateur, I.; Musiani, M. Determination of Effective Capacitance and Film Thickness from Constant-Phase-Element Parameters. *Electrochim. Acta* **2010**, *55* (21), 6218−6227.

DOI: 10.1021/acs.iecr.8b06306
Ind. Eng. Chem. Res. 2019, 58, 3033−3046